nature climate change

Analysis

https://doi.org/10.1038/s41558-023-01682-9

Coastal vegetation and estuaries are collectively a greenhouse gas sink

Received: 6 October 2022

Accepted: 21 April 2023

Published online: 22 May 2023



Judith A. Rosentreter \$\mathbb{0}^{1,2,3} \subseteq\$, Goulven G. Laruelle\$^4\$, Hermann W. Bange\$^5\$, Thomas S. Bianchi \$\mathbb{0}^6\$, Julius J. M. Busecke \$\mathbb{0}^7\$, Wei-Jun Cai \$\mathbb{0}^8\$, Bradley D. Eyre \$\mathbb{0}^1\$, Inke Forbrich \$\mathbb{0}^{9,10}\$, Eun Young Kwon \$\mathbb{0}^{11}\$, Taylor Maavara \$\mathbb{0}^{2,3,12}\$, Nils Moosdorf \$\mathbb{0}^{13,14,15}\$, Raymond G. Najjar \$\mathbb{0}^{16}\$, V. V. S. S. Sarma\$^{17}\$, Bryce Van Dam \$\mathbb{0}^{18}\$ & Pierre Regnier \$\mathbb{0}^4\$

Coastal ecosystems release or absorb carbon dioxide (CO_2), methane (CH_4) and nitrous oxide (N_2O), but the net effects of these ecosystems on the radiative balance remain unknown. We compiled a dataset of observations from 738 sites from studies published between 1975 and 2020 to quantify CO_2 , CH_4 and N_2O fluxes in estuaries and coastal vegetation in ten global regions. We show that the CO_2 -equivalent (CO_2 e) uptake by coastal vegetation is decreased by 23–27% due to estuarine CO_2 e outgassing, resulting in a global median net sink of 391 or 444 $TgCO_2$ e yr^{-1} using the 20- or 100-year global warming potentials, respectively. Globally, total coastal CH_4 and N_2O emissions decrease the coastal CO_2 sink by 9–20%. Southeast Asia, North America and Africa are critical regional hotspots of CO_2 uptake while effectively reducing CO_3 uptake while effectively reducing CO_3 and CO_3 uptake CO_3 upta

Since the beginning of the industrial era, atmospheric concentrations of the GHGs carbon dioxide (CO₂), methane (CH₄) and nitrous oxide (N₂O) have increased by 47, 156 and 23%, respectively, and continue to increase at alarming rates due to anthropogenic activities, driving global warming¹. The global terrestrial CO₂ sink is diminished by biogenic CH₄ and N₂O emissions due to anthropogenic activities such as agriculture or biomass burning, which result in a shift of the terrestrial biosphere from a net CO₂ sink to a net GHG source². Globally, it is now clear that inland waters are an atmospheric GHG source^{3,4} while the GHG budget of coastal ecosystems is less certain. Located in the downstream portion of the land–ocean aquatic continuum (LOAC)⁵, estuaries receive

large amounts of terrestrial carbon and nitrogen through riverine and groundwater flows, but their carbon and nitrogen cycles are also tightly interconnected with coastal vegetated ecosystems and the coastal oceans and coastal vegetation are thus a complex spatial and temporal combination of GHG sources and sinks, which complicates the estimate of the net global warming effect and makes the implementation of efficient mitigation strategies difficult.

Estuaries (tidal systems/deltas, lagoons and fjords) and surrounding coastal vegetation (mangroves, salt marshes and seagrasses) are strongly interconnected but show remarkable variations in their

¹Center for Coastal Biogeochemistry, Faculty of Science and Engineering, Southern Cross University, Lismore, New South Wales, Australia. ²Yale Institute for Biospheric Studies, Yale University, New Haven, CT, USA. ³Yale School of the Environment, Yale University, New Haven, CT, USA. ⁴Biogeochemistry and Modelling of the Earth System (BGEOSYS), Department of Geosciences, Environment and Society, Université Libre de Bruxelles, Brussels, Belgium. ⁵Marine Biogeochemistry, Helmholtz Centre for Ocean Research Kiel, Kiel, Germany. ⁶Department of Geological Sciences, University of Florida, Gainesville, FL, USA. ⁷Lamont-Doherty Earth Observatory, Columbia University, Palisades, NY, USA. ⁸School of Marine Science and Policy, University of Delaware, Newark, DE, USA. ⁹Ecosystems Center, Marine Biological Laboratory, Woods Hole, MA, USA. ¹⁰Department of Environmental Sciences, University of Toledo, Toledo, OH, USA. ¹¹Center for Climate Physics, Institute for Basic Science, Busan, South Korea. ¹²School of Geography, University of Leeds, Leeds, United Kingdom. ¹³Leibniz Centre for Tropical Marine Research, Bremen, Germany. ¹⁴Kiel University, Kiel, Germany. ¹⁵Southern Cross GeoScience, Southern Cross University, Lismore, New South Wales, Australia. ¹⁶Department of Meteorology and Atmospheric Science, The Pennsylvania State University, University Park, PA, USA. ¹⁷CSIR-National Institute of Oceanography, Visakhapatnam, India. ¹⁸Department of Fluxes Across Interfaces, Institute of Carbon Cycles, Helmholtz-Zentrum Hereon, Geesthacht, Germany. ¹⁸Ce-mail: judith.rosentreter@scu.edu.au

Table 1 | Global estuary and coastal vegetation GHG fluxes

Ecosystem	CO ₂ Tg CO ₂ yr ⁻¹		CO ₂ Tg CO ₂ yr ⁻¹ CH ₄ Tg CH ₄ yr ⁻¹		CH ₄ Tg CO ₂ e yr ⁻¹ GWP ₂₀		CH ₄ Tg CO ₂ e yr ⁻¹ GWP ₁₀₀		N ₂ O Gg N ₂ O yr ⁻¹		N ₂ O Tg CO ₂ e yr ⁻¹ GWP ₂₀		N ₂ O Tg CO ₂ e yr ⁻¹ GWP ₁₀₀		
	Median	Q1-Q3	Median	Q1-Q3	Median	Q1-Q3	Median	Q1-Q3	Median	Q1-Q3	Model	Median	Q1-Q3	Median	Q1-Q3
Global estuaries	111.1	72.7- 170.3	0.25	0.07- 0.46	19.6	5.45- 36.9	6.63	1.85- 12.5	61.3	41.4- 93.8	94.4	16.7	11.3-25.6	16.7	11.3- 25.6
Tidal systems and deltas	126.6	89.9– 175.5	0.14	0.11- 0.23	10.8	8.66- 18.1	3.66	2.94- 6.13	35.1	23.6- 48.4	49.8	9.58	6.45– 13.2	9.58	6.45– 13.2
Lagoons	50.0	27.8- 80.5	0.11	0.05- 0.13	8.53	4.15- 10.1	2.89	1.41- 3.43	9.93	6.24- 13.8	14.1	2.71	1.70- 3.76	2.71	1.70- 3.76
Fjords	-65.6	-96.4- -23.5	0.003	0.002- 0.008	0.25	0.15- 0.62	0.08	0.05- 0.21	16.3	11.8- 20.6	30.5	4.46	3.21–5.61	4.46	3.21- 5.61
Global coastal vegetation	-600.6	-773.5- -426.2	0.76	0.47- 1.41	60.8	37.4- 112.5	20.6	12.7- 38.1	6.34	0.70- 18.3		1.73	0.19– 5.00	1.73	0.19- 5.00
Mangroves	-359.3	-433.5- -333.4	0.34	0.21- 0.50	26.8	16.4- 39.8	9.07	5.57- 13.5	8.85	4.36- 19.3		2.42	1.19-5.27	2.42	1.19- 5.27
Salt marshes	-49.6	-59.0- -41.2	0.26	0.14- 0.36	20.3	11.2- 28.3	6.89	3.80- 9.60	2.06	-0.83- 6.08		0.56	-0.23- 1.66	0.56	-0.23- 1.66
Seagrasses	-191.6	-353.5- -53.2	0.17	0.09- 0.21	13.7	7.04- 16.9	4.64	2.38- 5.73	-4.56	-5.98- -3.39		-1.25	-1.63- -0.93	-1.25	-1.63- -0.93
Global estuaries + coastal vegetation	-489.5	-700.8- -255.9	1.01	0.54– 1.87	80.4	42.9- 149.4	27.2	14.5- 50.6	67.7	42.1- 112.1		18.5	11.5- 30.6	18.5	11.5- 30.6

Global median and Q1 to Q3 estuary (tidal systems/deltas, lagoons and fjords) and coastal vegetation (mangroves, salt marshes and seagrasses) CO_2 , CH_4 , N_2O and CO_2e GHG fluxes using the GWP_{2O} and GWP_{1O} time periods. Estuary N_2O fluxes are also shown based on the mechanistic model by Maavara et al. ²⁵.

magnitude and direction (sink or source) of GHG fluxes. Estuaries have been estimated to emit 0.4-2.2 PgCO₂ yr⁻¹ globally⁷⁻¹⁰, whereas mangroves and salt marshes collectively take up 0.3-1.7 PgCO₂ yr⁻¹ (Supplementary Table 1)5,8. Together with submergent seagrasses, coastal vegetation potentially store 304 (131-466) TgCO₂ yr⁻¹ of so-called blue carbon in their sediments^{11,12}. In contrast, emissions of CH₄ and N₂O from coastal sediments and surrounding waters can reduce some of the coastal vegetation carbon sinks^{13,14}, thereby complicating blue carbon assessments^{15,16}. A recent global synthesis showed that median CH₄ emissions from combined mangroves, salt marshes and seagrasses $(0.52 \, \text{TgCH}_4 \, \text{yr}^{-1})$ exceed those from estuaries $(0.23 \, \text{TgCH}_4 \, \text{yr}^{-1})^{17}$. However, CH₄ fluxes are highly variable across time and space, causing a large range in global estimates of both coastal vegetation (0.02- $6.20 \, \text{TgCH}_4 \, \text{yr}^{-1})^{17,18}$ and estuaries $(0.02-6.60 \, \text{TgCH}_4 \, \text{yr}^{-1})^{4,19}$ (Supplementary Table 2). Coastal N2O fluxes are less understood and it remains unclear whether coastal vegetated ecosystems are a net source or sink of N₂O to the atmosphere 20,21. Global estimates of estuarine N₂O emissions are highly uncertain, with large discrepancies for both observation-based (220-5,710 GgN₂O yr⁻¹)^{4,22,23} and modelling approaches (94–1,084 GgN₂O yr⁻¹)^{24,25} (Supplementary Table 3).

Here we present a data-driven meta-analysis synthesizing CO_2 , CH_4 and N_2O fluxes in three major estuary types (tidal systems/deltas, lagoons and fjords) and three coastal vegetation types (mangroves, salt marshes and seagrasses), both globally and in ten world regions. These regions were delineated by the Regional Carbon Cycle Assessment and Processes Phase 2 (RECCAP2) project²⁶—an activity of the Global Carbon Project. We compiled water—air CO_2 , CH_4 and N_2O fluxes for estuaries and combined CO_2 fluxes from eddy covariance with CH_4 and N_2O fluxes at the interfaces of water, sediments and plants with the atmosphere for coastal vegetation. Our dataset compiles observations from a total of 738 sites from studies published between 1975 and the end of 2020, and we provide a GHG flux climatology assumed to be representative for this period. The GHG fluxes are regionalized by combining GHG flux densities with recently published surface areas of

coastal vegetation $^{27-29}$ and estuaries 30 . As such, our global-scale regional assessment applies a consistent framework for all three GHGs and ecosystems. Regional GHG fluxes are then summed to provide global net GHG fluxes for estuaries, coastal vegetation and both systems combined. We quantify the net contemporary GHG radiative balance in units of CO_2 equivalents (CO_2 e) based on the global warming potential (GWP) of each gas for the 2O-year (GWP $_{20}$) and 1OO-year (GWP $_{100}$) time horizons 1 . Note that our study does not include an analysis of temporal changes in GHG fluxes required to assess a contribution to radiative forcing. Following the RECCAP2 regional segmentation, our coastal GHG budget can be integrated into broader budgets of continents.

Estuarine and coastal vegetation CO₂ fluxes

We estimate global median (first (Q1) to third(Q3)) CO₂ emissions from estuaries to be 111 (73-170) TgCO₂ yr⁻¹ (Table 1), which is three to five times lower (as is our mean of 121 TgCO₂ yr⁻¹) than recent mean estimates (370–550 TgCO₂ yr⁻¹)^{9,10}. Our lower global emissions are due to the inclusion of estuarine surface area³⁰ (Extended Data Fig. 1), that is, ~30% lower than previously estimated 31,32 , and include more sites than previous studies 9,10 . In particular, CO₂ flux data in fjords have more than doubled since earlier reviews^{8,10} that considered fjords as minimal CO₂ sources. In this Analysis, we show that fjords take up 66 (96-24) TgCO₂ yr⁻¹ from the atmosphere, reducing 37% of the CO₂ emissions from global tidal systems/deltas (127 (90-176) TgCO₂ yr⁻¹) and lagoons (50 (28-81) TgCO₂ yr⁻¹) (Fig. 1). Tidal systems and deltas, which account for 40% of the global estuarine surface area (Supplementary Table 4), show higher CO₂ flux densities than lagoons and fjords $(Supplementary\,Table\,5), probably\,due\,to\,their\,strong\,hydrological$ connectivity with rivers and groundwater that import CO₂ supersaturated waters³³. In addition, the considerably strong influence of tides³¹ can increase water turbulence and therefore gas transfer velocities³⁴, which in turn enhance CO₂ evasion from tidal systems. At the regional scale, we find distinct trends of CO₂ fluxes between different geomorphic estuary types (Fig. 1). For example, North America is a hotspot for

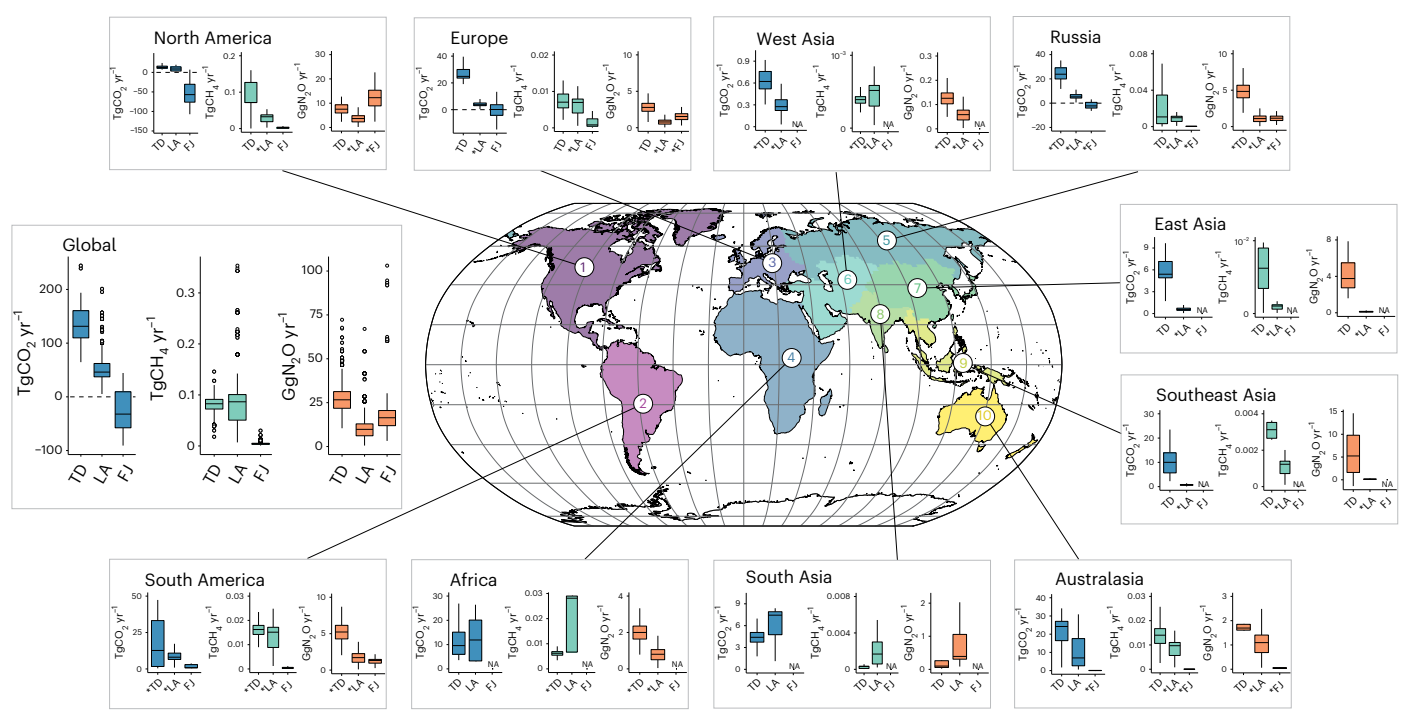


Fig. 1| **Regional and global estuary GHG fluxes.** The box and whisker plots show the median and interquartile (Q1–Q3) range of CO_2 , CH_4 and N_2O fluxes in tidal systems/deltas (TD), lagoons (LA) and fjords (FJ) in ten RECCAP2 regions and globally. A positive value indicates a flux from the ecosystem to the atmosphere

and a negative value indicates a flux from the atmosphere to the ecosystem. Outliers (open circles) are shown only for the global plots. Asterisks indicate that the flux was upscaled based on global statistics (n < 3) (see Methods). NA, not applicable.

atmospheric CO_2 uptake by fjords (57 (76–30) $TgCO_2$ yr⁻¹; 86% of the CO_2 uptake by global fjords). Long stretches of lagoons can be found along Africa's coastline that contribute 24% to global lagoon CO_2 emissions. Europe accounts for 20% of global CO_2 emissions by tidal systems and deltas, although it only comprises 5% of the total surface area of this estuary type. This disproportionate contribution stems from the highest median CO_2 flux densities (4.8 gCO_2 m⁻² d⁻¹) of any estuary type or region (Supplementary Table 5), probably fuelled by organic carbon loads from European rivers under strong anthropogenic pressure³⁵. European estuaries were over-represented in previous global analyses $^{9.10,36}$, which probably led to overestimates in global CO_2 emissions from estuaries.

Using data exclusively from eddy covariance long-term studies, we estimate that salt marshes, mangroves and seagrasses worldwide take up 601 (774–426) $TgCO_2\,yr^{-1}$ from the atmosphere—a flux that in absolute terms is more than five times greater than the estuarine CO_2 outgassing (Table 1). Our global estimate is lower but within the uncertainty range of a recent estimate of $843\pm440\,TgCO_2\,yr^{-1}$ by mangroves, salt marshes and seagrasses 5 . Note that our estimate of CO_2 uptake by coastal vegetation should be distinguished from carbon sequestration by coastal vegetation, which has been estimated to be $110-257\,TgCO_2\,yr^{-1}(ref.\,37)$ —roughly one-third of the $CO_2\,uptake$ —the remainder of which results in a lateral export of carbon, a substantial fraction of which can be transported over long distances to the open ocean 5 .

Seagrass meadows can be found in tropical, subtropical and temperate–cold climate zones. Mangroves are only abundant in subtropical and tropical climates, whereas salt marshes dominate in temperate regions (Extended Data Figs. 1 and 2). Highly productive mangrove forests³⁸ contribute the majority (60%) of the global CO₂ uptake by coastal vegetation (359 (434–333) TgCO₂ yr⁻¹). Globally, seagrasses (192 (354–53) TgCO₂ yr⁻¹) have around four times higher CO₂ uptake than salt marshes (50 (59–41) TgCO₂ yr⁻¹) (Fig. 2), which is similar to previous findings based on net primary production³⁹.

Since mangrove forests are abundant in tropical Southeast Asia, we find that this region contributes 37% to global mangrove CO_2 uptake, followed by Africa (20%) and tropical North and South America (both ~15%). Salt marshes are abundant along the west and east coasts of Canada and the United States. Therefore, North America contributes 34% of the global salt marsh CO_2 uptake. Other regions that provide a substantial salt marsh CO_2 sink include East Asia (23%) and Australasia (21%). Africa's coastline has the greatest contribution (24%) to global seagrass CO_2 uptake.

Estuarine and coastal vegetation CH₄ fluxes

Global estuaries emit 0.25 (0.07-0.46) TgCH₄ yr⁻¹ (Table 1)—a median value that falls at the lower end of the range of previous assessments^{4,19,40} (Supplementary Table 2), yet is close to the recent median estimate (0.23 (0.02–0.91) TgCH₄ yr⁻¹) by Rosentreter et al. ¹⁷. Global estuarine CH₄ emissions are dominated by tidal systems/deltas (0.14 (0.11–0.23) $TgCH_4 yr^{-1}$; 56%) and lagoons (0.11 (0.05–0.13) $TgCH_4 yr^{-1}$; 44%), while fjords contribute <1%. Our regional analysis shows that North America's tidal systems and deltas contribute the majority (50%) of global CH₄ emissions from this estuary type (Fig. 1). North America also shows the highest median CH₄ flux densities (2.9 mgCH₄ m⁻² d⁻¹) of tidal systems and deltas, particularly in the United States, where many eutrophic systems undergo seasonal hypoxia or anoxia that fuels CH₄ production⁴¹ (Supplementary Table 6). South America, Russia and Australasia contribute ~10% each to global CH₄ emissions from tidal systems and deltas, whereas all other regions are minor contributors (<5%). North America comprises the largest area of lagoons (Extended Data Fig. 1), thereby dominating global lagoonal CH₄ emissions (30%). Other regions with substantial lagoon CH₄ emissions are Africa (25%) and South America (14%), whereas the remaining regions contribute <10%. Interestingly, we find that of all of the estuary types and regions, lagoons in Africa show the highest flux density (5.3 mgCH₄ m⁻² d⁻¹), driven by high CH₄ production in anoxic bottom waters in permanently stratified lagoons along the Ivory Coast⁴².

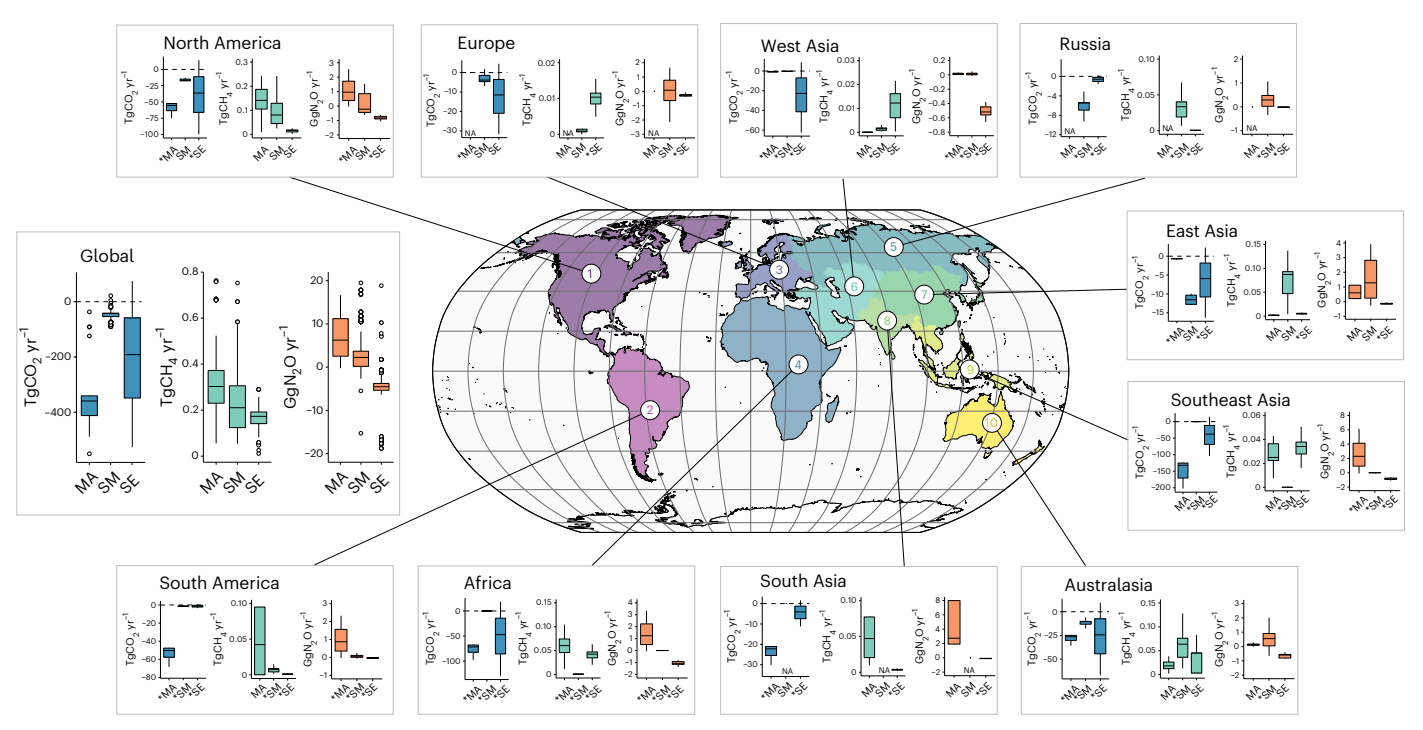


Fig. 2 | **Regional and global coastal vegetation GHG fluxes.** The box and whisker plots show the median and interquartile (Q1–Q3) range of CO₂, CH₄ and N₂O fluxes in mangroves (MA), salt marshes (SM) and seagrasses (SE) in ten RECCAP2 regions and globally. A positive value indicates a flux from the

ecosystem to the atmosphere (emission) and a negative value indicates a flux from the atmosphere to the ecosystem (uptake). Outliers (open circles) are shown only for the global plots. Asterisks indicate that the flux was upscaled based on global statistics (n < 3) (see Methods). NA, not applicable.

Globally, mangroves, salt marshes and seagrasses combined release 0.76 (0.47–1.41) TgCH₄ yr⁻¹, which is more than three times the CH₄ released by global estuaries. Our coastal vegetation estimate is comparable to that reported in a recent review¹⁷ but incorporates more data, resulting in an increased estimate for salt marshes and mangroves but not seagrasses. We find that mangroves (0.34 (0.21–0.50) TgCH₄ yr⁻¹) dominate coastal vegetation CH₄ emissions, followed by salt marshes $(0.26 (0.14-0.36) \text{ TgCH}_4 \text{ yr}^{-1})$ and seagrasses (0.17 (0.09-0.21)TgCH₄ yr⁻¹) (Table 1 and Fig. 2). The high CH₄ emissions from mangroves (exceeding global estuaries) are promoted by carbon-rich deep anoxic sediments⁴³ and tidally induced mixing between groundwater rich in CH₄ and surface waters⁴⁴. We find the highest mangrove CH₄ flux densities (21 mgCH₄ m⁻² d⁻¹) in East Asia. However, North America's mangrove forests dominate (41%) global mangrove CH₄ emissions because its forest area is 86 times greater than in East Asia and the CH₄ flux density is similarly high (Supplementary Table 6). Globally, Southeast Asia comprises most of the mangrove forest area, but the region's much lower CH₄ flux density (1.4 mgCH₄ m⁻² d⁻¹) means that it adds only 6% to global mangrove CH₄ emissions. Such a low regional evasion rate may be explained by high monsoonal rainfall events and short water residence times, resulting in low rates of anaerobic organic matter decomposition⁴⁵. The highest median CH₄ flux densities of any coastal vegetation type are found in East Asian salt marshes (44 mgCH₄ m⁻² d⁻¹), with this region contributing 34% of global salt marsh CH₄ emissions despite its relatively small marsh coverage. North America's vast salt marsh areas are the second highest contributor (35%) to global salt marsh emissions. Australasia's seagrass meadows dominate (29%) global seagrass CH₄ emissions due to a combination of moderately high seagrass area and a regional flux density that is more than twice the global median (Supplementary Table 6).

Estuarine and coastal vegetation N₂O fluxes

We estimate that estuaries globally emit 61(41-94) GgN₂O yr⁻¹ (Table 1), which is substantially lower than previous observational and modelling

estimates (94-5,710 GgN₂O yr⁻¹)^{4,24,25,46} (Supplementary Table 3). Similar to CO₂ and CH₄, our lower estuary N₂O emissions are partially due to the lower estuarine surface area used in this study³⁰, but also reflect the ~80% more sites in our analysis than earlier reviews^{23,46}. We find the highest N₂O emissions in tidal systems and deltas (35 (24–48) GgN₂O yr⁻¹), but in contrast with CO₂ and CH₄, fjords are the second highest N₂O emitter (16 (12-21) GgN₂O yr⁻¹)—almost double that of lagoons (10 (6–14) GgN₂O yr⁻¹). Regionally, North America contributes 27, 37 and 77% to global emissions from tidal systems/deltas, lagoons and fiords, respectively, contributing 25 (15–46) GgN₂O yr⁻¹ (41%) to global estuary N₂O emissions (Fig. 1). Other regions of moderate emissions are South America (14%), Russia (12%) and Southeast Asia (9%), with the remaining regions being only minor contributors (<5 GgN₂O vr⁻¹). We further compare our data-driven approach with the recently published mechanistic model of global estuary N₂O emissions²⁵ that was regionalized for comparison purposes. The modelled global emission estimates from all three estuary types (94 GgN₂O yr⁻¹) fall close to the upper uncertainty bound reported in our study. As such, we find an overall good agreement between the two approaches. Fjord emissions represent the largest relative difference between modelled and data-driven estimates (Table 1).

Coastal vegetation can be a source or sink of N_2O to the atmosphere. We find that emissions slightly exceed uptake at the global scale, resulting in 6.3 (0.7–18.3) GgN_2O yr⁻¹, which is only -10% that of estuaries (Table 1). Globally, mangroves emit 8.9 (4.4–19.3) GgN_2O yr⁻¹, more than four times that of salt marshes (2.1 (–0.8–6.1) GgN_2O yr⁻¹). Seagrasses take up 4.6 (6.0–3.4) GgN_2O yr⁻¹, thereby offsetting almost half of the N_2O emitted by salt marshes and mangroves (Fig. 2). Nevertheless, large variability can be found in local N_2O fluxes in coastal vegetation. For example, current studies report N_2O uptake from salt marshes in North America⁴⁷ and Europe⁴⁸, while studies from East Asia, mainly China, reveal that this region accounts for a substantial 1.3 (0.2–2.8) GgN_2O yr⁻¹ (62%) of global salt marsh emissions. Mangrove ecosystems are generally a source of N_2O , although some mangrove

Table 2 | Regional coastal CO2e GHG fluxes

Region		Estuari	Coastal vegetation				Estuaries and coastal vegetation					
	TgCO ₂ eyr ⁻¹ for GWP ₂₀		TgCO₂eyr ⁻¹ for GWP ₁₀₀		TgCO ₂ eyr ⁻¹ for GWP ₂₀		TgCO ₂ eyr ⁻¹ for GWP ₁₀₀		TgCO ₂ eyr ⁻¹ for GWP ₂₀)		TgCO₂eyr ⁻¹ for GWP ₁₀₀	
	Median	Q1 to Q3	Median	Q1 to Q3	Median	Q1 to Q3	Median	Q1 to Q3	Median	Q1 to Q3	Median	Q1 to Q3
North America	-20.1	-33.6 to -5.97	-25.7	-33.9 to -12.1	-89.4	-123.9 to -43.0	-102.0	-131.2 to -64.6	-109.6	-157.5 to -49.0	-127.7	-165.1 to -76.7
South America	13.3	7.68 to 26.1	11.6	6.54 to 22.7	-48.5	-66.1 to -26.9	-51.1	-66.1 to -32.8	-35.3	-58.4 to -0.79	-39.5	-59.5 to -10.1
Europe	31.3	28.5 to 36.2	30.5	27.9 to 34.9	-14.5	-19.5 to -5.72	-15.1	-19.9 to -6.46	16.8	8.98 to 30.5	15.4	8.07 to 28.5
Africa	25.1	13.4 to 44.9	23.3	13.4 to 37.3	-110.5	-143.4 to -56.6	-116.0	-147.1 to -73.4	-85.4	-130.0 to -11.7	-92.6	-133.8 to -36.1
Russia	30.4	25.7 to 41.8	29.3	25.4 to 38.2	-3.77	-6.08 to -1.17	-5.23	-7.05 to -3.04	26.6	19.6 to 40.6	24.1	18.3 to 35.2
West Asia	1.02	0.91 to 1.28	0.97	0.86 to 1.23	-22.8	-29.4 to -12.7	-23.5	-29.8 to -15.1	-21.8	-28.5 to -11.4	-22.5	-28.9 to -13.9
East Asia	7.59	6.24 to 10.4	7.21	6.03 to 9.80	-10.1	-18.0 to -3.09	-15.1	-21.8 to -9.81	-2.51	-11.8 to 7.27	-7.88	-15.8 to -0.01
South Asia	12.6	10.6 to 13.9	12.5	10.5 to 13.8	-21.5	-30.7 to -8.48	-24.2	-31.9 to -13.5	-8.93	−20.1 to 5.47	-11.7	-21.4 to 0.34
Southeast Asia	12.5	7.97 to 21.4	12.3	7.78 to 21.2	-164.9	-229.2 to -122.8	-168.0	-231.5 to -127.0	-152.4	-221.2 to -101.4	-155.8	-223.7 to -105.8
Australasia	33.7	22.1 to 42.8	32.5	21.4 to 41.4	-51.9	-69.7 to -28.2	-58.0	-74.3 to -37.4	-18.2	-47.6 to 14.6	-25.5	-53.0 to 3.95
Global	147.4	89.5 to 232.8	134.5	85.9 to 208.4	-538.0	-735.9 to -308.7	-578.2	-760.7 to -383.1	-390.6	-646.5 to -75.8	-443.8	-674.8 to -174.6

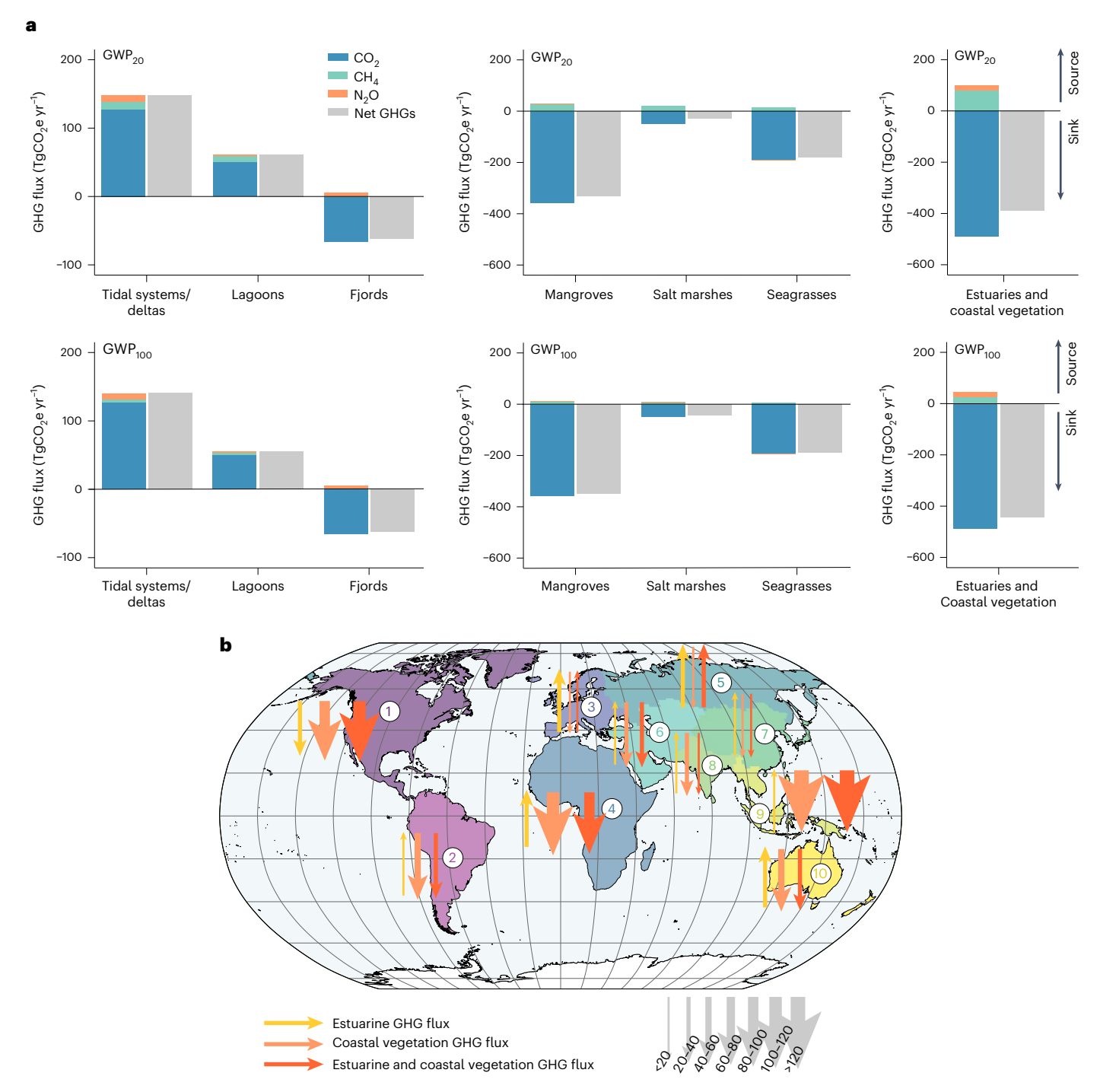
Median and Q1 to Q3 estuary and coastal vegetation CO_2e GHG fluxes using GWP_{20} and GWP_{100} . Negative values indicate net uptake of GHGs from the atmosphere and positive values indicate net release of GHGs to the atmosphere.

creeks in Australia have been shown to consume N_2O due to low nitrogen concentrations^{20,21}. Our seagrass N_2O flux database is strongly biased towards data from Australia, where studies mostly suggest N_2O uptake from near-pristine seagrasses⁴⁹ (Supplementary Table 7).

Implication for regional and global budgets

Our data-driven meta-analysis reveals that estuarine CO₂e GHG emissions reduce the coastal vegetation CO₂e GHG uptake by 27% (using GWP₂₀) or 23% (using GWP₁₀₀). Therefore, estuaries and coastal vegetation are collectively a GHG sink for the atmosphere of 391 (647–76) $TgCO_2e yr^{-1} or 444 (675-175) TgCO_2e yr^{-1} based on the GWP_{20} or GWP_{100}$ respectively (Table 2 and Fig. 3). Our quantification of the net GHG sink is broadly consistent with previous assessments based solely on CO₂^{5,7,8}. However, we find that this sink results both from a downward revision of coastal vegetation CO₂ fixation and substantially lower estuarine GHG outgassing, mostly due to the CO₂ uptake by fjords and a reduced estuarine surface area³⁰. The net CO₂ sink of estuaries and coastal vegetation is also substantially compensated by CH₄ and N₂O emissions, which offset 20 and 9% for the GWP₂₀ and GWP₁₀₀, respectively. Our global-scale assessment considerably reduces the uncertainty in the contemporary GHG budget⁵ and emphasizes that the combined contribution of coastal vegetation and estuaries to the global radiative balance is a cooling effect, in contrast with terrestrial sources² and inland waters^{3,4} (Fig. 4). However, our analysis does not address whether human activity has changed the radiative balance of these systems since the pre-industrial period. Importantly, we reveal where estuarine fluxes enhance, partially reduce or exceed coastal vegetation CO₂ uptake, allowing us to identify regional hotspots of GHG uptake and release (Fig. 3). We find that eight out of ten coastal regions are a net GHG sink for the atmosphere, regardless of the time horizon considered (Table 2). Using GWP₁₀₀, Southeast Asia shows the greatest net GHG sink (156 (224–106) TgCO₂e yr⁻¹) because of its extensive and highly productive tropical mangrove forests and seagrass meadows (Extended Data Fig. 1), as well as its accommodation of relatively few estuaries compared with other regions³⁰. A second regional hotspot for GHG sinks is North America (128 (165–77) TgCO₂e yr⁻¹) due to its expansive mangrove, salt marsh and seagrass areas, as well as its incorporation of the largest area of CO₂-absorbing fjords globally (40% of which are located in Greenland). In Africa, the large CO₂ uptake by coastal vegetation is partially offset by estuarine GHG outgassing, leaving Africa as the third greatest net GHG sink (93 (134–36) TgCO₂e yr⁻¹) globally. Australasia and West Asia are moderate GHG sinks (both ~25 TgCO₂e yr⁻¹), while in East and South Asia, coastal vegetation CO₂ sinks are largely offset by estuarine GHG release, resulting in a combined small net GHG sink of <20 TgCO₂e yr⁻¹. In Europe and Russia, estuarine GHG outgassing across a large estuarine surface area exceeds uptake from the relatively small area of coastal vegetation, making these regions net GHG sources. As such, our regionalized assessment suggests that, in addition to being a net global sink of GHGs for the atmosphere, the sink attributed to estuaries and coastal vegetation is also a common feature in many regions across the world.

The limitations of our GHG synthesis fall largely into four categories: the mapping of ecosystems; GHG flux measurements; spatio-temporal variability; and coupling between coastal vegetation and estuaries. The tidal marsh area used in this study²⁹ is probably underestimated due to the recent surge in restoration efforts resulting in a gain in tidal marsh area⁵⁰ and the lack of global mapping of freshwater tidal marshes. We exclude low-salinity (<0.5) tidal river GHG fluxes because of the difficulty in separating these from non-tidal rivers and because the biogeochemistry and residence times are distinctly different from those of brackish estuaries¹⁹. Our coastal GHG budget is focused on the interface of the atmosphere with coastal vegetation and estuaries. We do not account for other



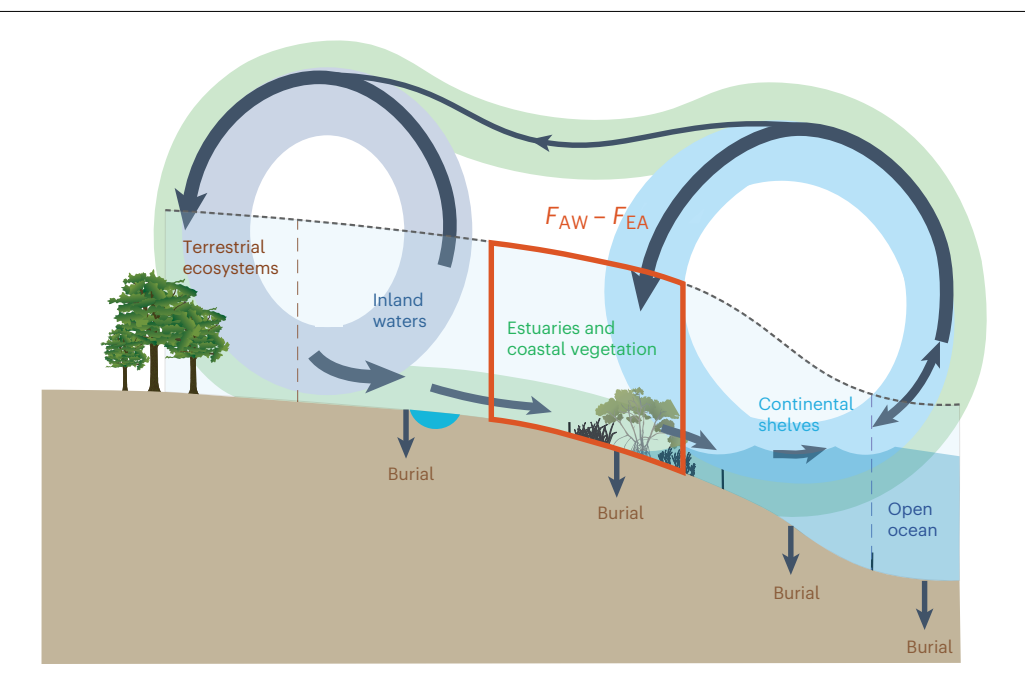
 $\label{eq:Fig.3} I \ Global \ and \ regional \ coastal \ CO_2e \ GHG \ fluxes. \ a, \ Global \ median \ GHG \ sources \ and \ sinks \ of \ estuaries \ and \ coastal \ vegetation \ using \ the \ GWP_{20} (top) \ and \ GWP_{100} (bottom) \ time \ horizons. \ The \ radiative \ balance \ is \ expressed \ in \ TgCO_2e \ yr^1 \ for \ CO_2, \ CH_4, \ N_2O \ and \ their \ sum \ (net \ GHGs). \ b, \ Conceptual \ diagram \ showing \ the \ magnitude \ of \ the \ CO_2e \ GHG \ fluxes \ for \ estuaries, \ coastal \ vegetation \ and \ their$

sum in the ten RECCAP2 regions and relative to each other. The size of each arrow is proportional to the flux in $TgCO_2e$ yr 1 (Table 2). The arrow sizes are the same for GWP_{20} and GWP_{100} : therefore arrows are not shown for the two GWP time horizons individually.

radiative effects that may arise from lateral transport, such as offsite emissions or blue carbon burial in marine sediments. The ebullitive and plant-mediated $\mathrm{CH_4}$ flux is under-represented in our analysis due to the scarcity of such data. Despite recent progress, GHG flux measurements are still lacking, particularly from Africa, Russia and West Asia. To better capture temporal variability, eddy covariance towers and conventional time series measurements are needed, even in regions with good spatial coverage. High spatio-temporal

variability means that techniques such as remote sensing 50, empirical modelling and process-based modelling are needed for extrapolating flux densities and projecting future hotspots, particularly in the face of climate change and population growth along the coast. Coastal vegetation and estuaries are intimately coupled. However, the quantity and quality of material transported laterally and the fraction and mechanisms controlling outgassing through the coastal vegetation–estuary interface or further offshore are currently poorly

а



b

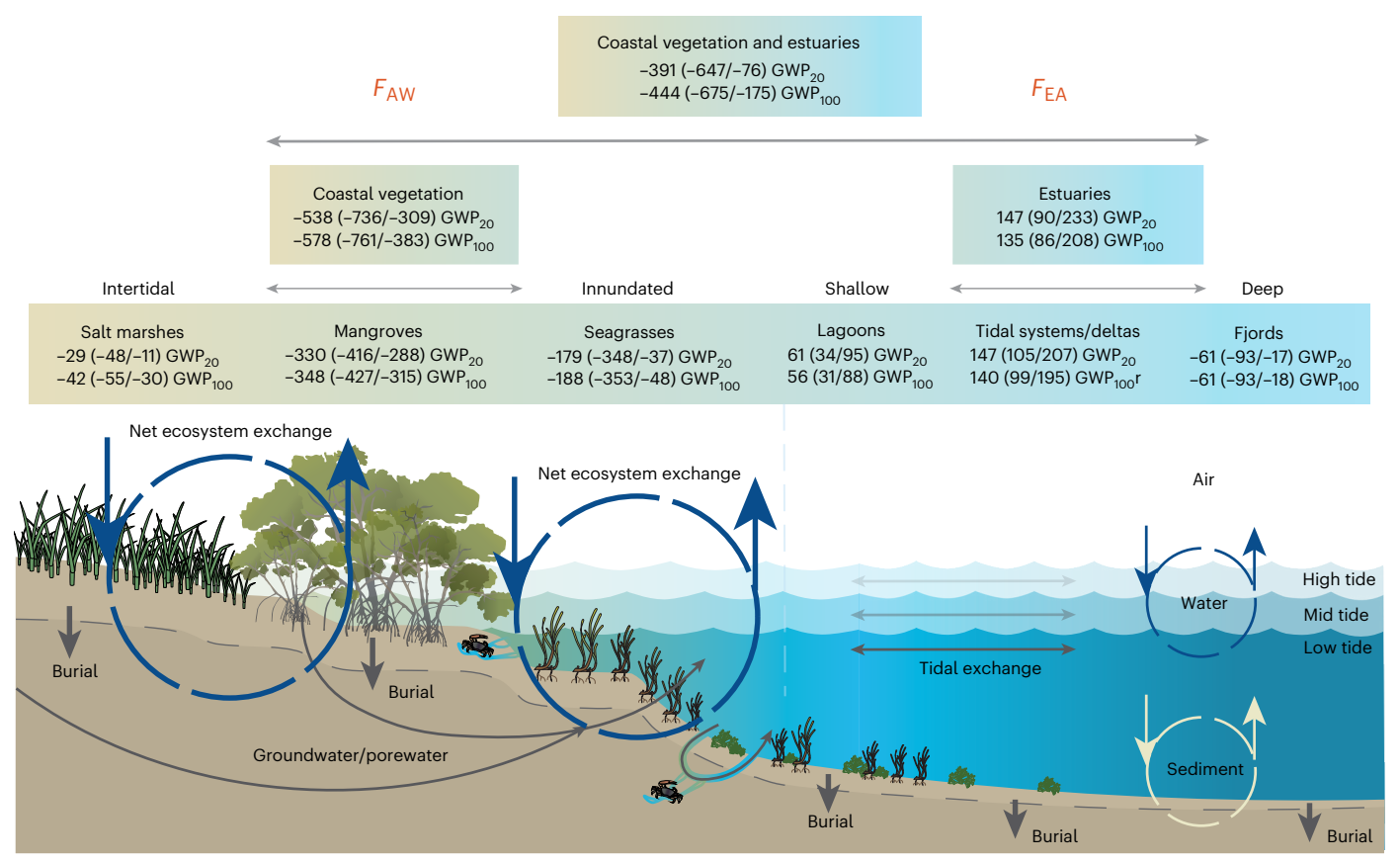


Fig. 4 | **Estuary and coastal vegetation GHG fluxes in the LOAC.** a, LOAC carbon loop model. The green loop connects the terra firme ecosystems to the open ocean. The two shorter loops connect the terra firme ecosystems to inland waters (grey) and the coastal vegetation, estuaries and continental shelves to the open ocean (blue). F_{AW} represents GHG fluxes by tidal wetlands (salt marshes and mangroves) and submerged vegetation, whereas F_{EA} represents estuarine GHG

fluxes. **b**, Global median (Q1/Q3) CO $_2$ e GHG fluxes in coastal vegetation and in estuaries, using the GWP $_{20}$ and GWP $_{100}$ time horizons. Here we include seagrasses in coastal vegetation fluxes (F_{AW}), whereas Regnier et al. 5 separated seagrasses as submerged vegetation from intertidal emergent mangroves and salt marshes. Units are in TgCO $_2$ e yr 1 . Panel **a** adapted with permission from ref. 5, Springer Nature Limited.

known⁵¹, particularly for CH_4 and N_2O . Despite its limitations, our coastal GHG synthesis addresses the current research gap between local and global scales and identifies regional hotspots. The future

role of coastal ecosystems as a sink or source of GHGs in each world region will depend on the adoption of best practices to reduce CH₄ and N₂O emissions while strengthening CO₂ uptake.

Online content

Any methods, additional references, Nature Portfolio reporting summaries, source data, extended data, supplementary information, acknowledgements, peer review information; details of author contributions and competing interests; and statements of data and code availability are available at https://doi.org/10.1038/s41558-023-01682-9.

References

- IPCC Climate Change 2021: The Physical Science Basis (eds Masson-Delmotte, V. et al.) (Cambridge Univ. Press, 2021).
- Tian, H. et al. The terrestrial biosphere as a net source of greenhouse gases to the atmosphere. Nature 531, 225–228 (2016).
- Raymond, P. A. et al. Global carbon dioxide emissions from inland waters. Nature 503, 355–359 (2013).
- Zheng, Y. et al. Global methane and nitrous oxide emissions from inland waters and estuaries. Glob. Chang. Biol. 28, 4713–4725 (2022).
- Regnier, P., Resplandy, L., Najjar, R. G. & Ciais, P. The land-to-ocean loops of the global carbon cycle. Nature 603, 401–410 (2022).
- Abril, G. & Borges, A. V. Ideas and perspectives: carbon leaks from flooded land: do we need to replumb the inland water active pipe? *Biogeosciences* 16, 769–784 (2019).
- Cai, W.-J. Estuarine and coastal ocean carbon paradox: CO₂ sinks or sites of terrestrial carbon incineration? Ann. Rev. Mar. Sci. 3, 123–145 (2011).
- Bauer, J. E. et al. The changing carbon cycle of the coastal ocean. Nature 504, 61-70 (2013).
- Chen, C. T. A. et al. Air–sea exchanges of CO₂ in the world's coastal seas. *Biogeosciences* 10, 6509–6544 (2013).
- Laruelle, G. G. et al. Global multi-scale segmentation of continental and coastal waters from the watersheds to the continental margins. *Hydrol. Earth Syst. Sci.* 17, 2029–2051 (2013).
- 11. Macreadie, P. I. et al. Blue carbon as a natural climate solution. Nat. Rev. Earth Environ. **2**, 826–839 (2021).
- Gattuso, J.-P., Williamson, P., Duarte, C. M. & Magnan, A. K. The potential for ocean-based climate action: negative emissions technologies and beyond. Front. Clim. 2, 575716 (2021).
- Rosentreter, J. A., Maher, D. T., Erler, D. V., Murray, R. H. & Eyre,
 B. D. Methane emissions partially offset "blue carbon" burial in mangroves. Sci. Adv. 4, eaao4985 (2018).
- 14. Oreska, M. P. J. et al. The greenhouse gas offset potential from seagrass restoration. *Sci. Rep.* **10**, 7325 (2020).
- Rosentreter, J. A., Al-Haj, A. N., Fulweiler, R. W. & Williamson, P. Methane and nitrous oxide emissions complicate coastal blue carbon assessments. Glob. Biogeochem. Cycles 35, e2020GB006858 (2021).
- Williamson, P. & Gattuso, J. Carbon removal using coastal blue carbon ecosystems is uncertain and unreliable, with questionable climatic cost-effectiveness. Front. Clim. 4, 853666 (2022).
- Rosentreter, J. A. et al. Half of global methane emissions come from highly variable aquatic ecosystem sources. *Nat. Geosci.* 14, 225–230 (2021).
- Al-Haj, A. N. & Fulweiler, R. W. A synthesis of methane emissions from shallow vegetated coastal ecosystems. *Glob. Change Biol.* 26, 2988–3005 (2020).
- 19. Borges, A. V. & Abril, G. in *Treatise on Estuarine and Coastal Science* Vol. 5 119–161 (Elsevier, 2011).
- Maher, D. T., Sippo, J. Z., Tait, D. R., Holloway, C. & Santos, I. R. Pristine mangrove creek waters are a sink of nitrous oxide. Sci. Rep. 6, 25701 (2016).
- Murray, R., Erler, D., Rosentreter, J., Maher, D. & Eyre, B. A seasonal source and sink of nitrous oxide in mangroves: insights from concentration, isotope, and isotopomer measurements. Geochim. Cosmochim. Acta 238, 169–192 (2018).

- De Wilde, H. P. J. & De Bie, M. J. M. Nitrous oxide in the Schelde estuary: production by nitrification and emission to the atmosphere. *Mar. Chem.* 69, 203–216 (2000).
- 23. Murray, R. H., Erler, D. V. & Eyre, B. D. Nitrous oxide fluxes in estuarine environments: response to global change. *Glob. Change Biol.* **21**, 3219–3245 (2015).
- Kroeze, C., Dumont, E. & Seitzinger, S. Future trends in emissions of N₂O from rivers and estuaries. *J. Integr. Environ. Sci.* 7, 71–78 (2010).
- Maavara, T. et al. Nitrous oxide emissions from inland waters: are IPCC estimates too high? Glob. Change Biol. 25, 473–488 (2019).
- Ciais, P. et al. Definitions and methods to estimate regional land carbon fluxes for the second phase of the REgional Carbon Cycle Assessment and Processes Project (RECCAP-2). Geosci. Model Dev. 15, 1289–1316 (2020).
- 27. Bunting, P. et al. The Global Mangrove Watch—a new 2010 global baseline of mangrove extent. *Remote Sens.* **10**, 1669 (2018).
- 28. Mcowen, C. et al. A global map of saltmarshes (v6.1). *Biodivers. Data J.* **5**, e11764 (2017).
- Short, F. T. Global Distribution of Seagrasses (Version 6.0). Sixth Update to the Data Layer Used in Green and Short (2003). (UN Environment Programme World Conservation Monitoring Centre, 2017); https://data.unep-wcmc.org/datasets/7
- Laruelle, G. G., Rosentreter, J. A. & Regnier P. Extrapolation based regionalized re-evaluation of the global estuarine surface area. Preprint at *Earth ArXiv* https://doi.org/10.31223/X5X664 (2023).
- 31. Dürr, H. H. et al. Worldwide typology of nearshore coastal systems: defining the estuarine filter of river inputs to the oceans. *Estuaries Coasts* **34**, 441–458 (2011).
- 32. Woodwell, G. M., Rich, P. H. & Hall, C. A. S. in *Carbon and the Biosphere* (eds Woodwell, G. M. & Pecan, E. V.) 221–240 (Technical Information Center, United States Atomic Energy Commission & National Technical Information Service, 1973).
- Stewart, B. T., Santos, I. R., Tait, D. R., Macklin, P. A. & Maher, D. T. Submarine groundwater discharge and associated fluxes of alkalinity and dissolved carbon into Moreton Bay (Australia) estimated via radium isotopes. *Mar. Chem.* 174, 1–12 (2015).
- 34. Borges, A. V. et al. Variability of the gas transfer velocity of CO_2 in a macrotidal estuary (the Scheldt). *Estuaries* **27**, 593–603 (2004).
- Frankignoulle, M. Carbon dioxide emission from European estuaries. Science 282, 434–436 (1998).
- 36. Regnier, P. et al. Modelling estuarine biogeochemical dynamics: from the local to the global scale. *Aquat. Geochem.* **19**, 591–626 (2013).
- 37. Lovelock, C. E. & Reef, R. Variable impacts of climate change on blue carbon. *One Earth* **3**, 195–211 (2020).
- 38. Alongi, D. M. Carbon cycling and storage in mangrove forests. *Ann. Rev. Mar. Sci.* **6**, 195–219 (2014).
- 39. Alongi, D. M. Carbon balance in salt marsh and mangrove ecosystems: a global synthesis. *J. Mar. Sci. Eng.* **8**, 767 (2020).
- Bange, H. W., Bartell, U. H., Rapsomanikis, S. & Andreae, M. O. Methane in the Baltic and North Seas and a reassessment of the marine emissions of methane. *Glob. Biogeochem. Cycles* 8, 465–480 (1994).
- 41. Gelesh, L., Marshall, K., Boicourt, W. & Lapham, L. Methane concentrations increase in bottom waters during summertime anoxia in the highly eutrophic estuary, Chesapeake Bay, U.S.A. *Limnol. Oceanogr.* **61**, S253–S266 (2016).
- 42. Koné, Y. J. M., Abril, G., Delille, B. & Borges, A. V. Seasonal variability of methane in the rivers and lagoons of Ivory Coast (West Africa). *Biogeochemistry* **100**, 21–37 (2010).
- 43. Donato, D. C. et al. Mangroves among the most carbon-rich forests in the tropics. *Nat. Geosci.* **4**, 293–297 (2011).
- 44. Maher, D. T., Santos, I. R., Golsby-Smith, L., Gleeson, J. & Eyre, B. D. Groundwater-derived dissolved inorganic and organic carbon

- exports from a mangrove tidal creek: the missing mangrove carbon sink? *Limnol. Oceanogr.* **58**, 475–488 (2013).
- Rao, G. D. & Sarma, V. V. S. S. Variability in concentrations and fluxes of methane in the Indian estuaries. *Estuaries Coasts* 39, 1639–1650 (2016).
- 46. Bange, H. W., Rapsomanikis, S. & Andreae, M. O. The Aegean Sea as a source of atmospheric nitrous oxide and methane. *Mar. Chem.* **53**, 41–49 (1996).
- Chmura, G. L., Kellman, L., van Ardenne, L. & Guntenspergen, G. R. Greenhouse gas fluxes from salt marshes exposed to chronic nutrient enrichment. *PLoS ONE* 11, e0149937 (2016).
- Dausse, A. et al. Biogeochemical functioning of grazed estuarine tidal marshes along a salinity gradient. *Estuar. Coast. Shelf Sci.* 100, 83–92 (2012).
- 49. Chen, J., Wells, N. S., Erler, D. V. & Eyre, B. D. Land-use intensity increases benthic N_2O emissions across three sub-tropical estuaries. *J. Geophys. Res. Biogeosciences* **127**, e2022JG006899 (2022).

- 50. Murray, N. J. et al. High-resolution mapping of losses and gains of Earth's tidal wetlands. *Science* **376**, 744–749 (2022).
- 51. Shields, M. R. et al. Carbon storage in the Mississippi River delta enhanced by environmental engineering. *Nat. Geosci.* **10**, 846–851 (2017).

Publisher's note Springer Nature remains neutral with regard to jurisdictional claims in published maps and institutional affiliations.

Springer Nature or its licensor (e.g. a society or other partner) holds exclusive rights to this article under a publishing agreement with the author(s) or other rightsholder(s); author self-archiving of the accepted manuscript version of this article is solely governed by the terms of such publishing agreement and applicable law.

@ The Author(s), under exclusive licence to Springer Nature Limited 2023

Methods

Definitions of estuaries (tidal systems/deltas, lagoons and fjords) and coastal vegetation (mangroves, salt marshes and seagrasses) can be found in the Supplementary Information.

Estuarine surface areas

The estuarine surface areas used in this study were calculated using a novel regionalized approach that combines available national databases and an extrapolation method that derives the total estuarine surface area of a region from the surface areas of its largest systems³⁰. Using a well-established global coastal segmentation comprising 45 regions (Margins and Catchment Segmentation (MARCATS)¹⁰), a surface area was determined for each estuary type (tidal systems/deltas, lagoons or fiords) in each region. Wherever exhaustive regional or national databases were available and covered an entire MARCATS segment (that is, Australia, New Zealand and all lagoons surrounding the Mediterranean Sea), the type-specific surface areas were extracted from these databases by assigning each identified system to a given type. In other regions, the surface areas were extrapolated from the five to ten largest systems. The extrapolation method relies on the observation that the cumulative estuarine surface area expressed as a function of the number of estuaries ranked by decreasing size within a sufficiently large stretch of coastline can be fitted by an equation of the form $S = (a \times N)/(b + N)$, where S is the total estuarine surface area (in km²), N is the number of estuaries, and a and b are dimensionless calibration coefficients. Using several extensive national estuarine databases (Australia, New Zealand and the United States), it was shown that fitting the parameters of this generic formula using only the ten largest estuaries of a given region generally allows prediction of the total cumulative surface area of the region with 9% accuracy. This uncertainty due to extrapolation is complemented by an uncertainty associated with the accuracy in estimating the surface areas of the individual systems used to perform the calculations, which ranges from 4-15% depending on the estuary type. Within each MARCATS region, the surface areas of the ten largest systems of each estuary type were gathered from national databases (United Kingdom, Mexico, United States, Australia, South Africa and South Korea), regional surveys (Food and Agriculture Organization and United Nations Educational, Scientific and Cultural Organization) or the global database Sea Around Us or calculated individually using a geographic information system. These data were then sorted and fitted using the equation described above to derive the estuarine surface area for each MARCATS and each estuary type, and finally summed to obtain the area for each of the ten RECCAP2 regions. For further details, see Laruelle et al.30.

Coastal vegetation surface areas

For all three coastal vegetation types, we segmented the vegetation area given as a global collection of polygons²⁷⁻²⁹ into the larger MARCATS regions¹⁰ using the following approach. The MARCTAS regions were first converted from the raster format to polygons using the Python package rasterio⁵². To find the area of each coastal vegetation type within a given MARCATS region, we first dissolved overlapping individual polygons to avoid overestimation of the vegetation area. We found the union of each polygon and the larger MARCATS region and recalculated the area using the EPSG:6933 projection, using the Python package geopandas⁵³, and finally summed these values. The same process was repeated for each large-scale MARCATS region and coastal vegetation type individually. The available shapefiles for MARCATS regions were converted from gridded outputs to polygons using rasterio⁵². Using geopandas for each region, we dissolved overlapping polygons and calculated the area of each polygon within the region using the EPSG:6933 projection, and finally summed the area for each of the ten RECCAP2 regions.

Estuarine GHG fluxes

We estimated estuary water–air fluxes of CO_2 , CH_4 and N_2O based on data from peer-reviewed publications until the end of 2020. We conducted

a literature search in Google Scholar and data publishers (FLUXNET, PANGAEA. MEMENTO and the British Oceanographic Data Centre) using the search string '(CO₂ OR CH₄ OR N₂O) AND (tidal system OR delta OR lagoon OR fjord)'. Additionally, we scanned the reference lists of publications. For each site/study location (>10 km apart), we averaged spatial and seasonal variation to a single water-air flux density, resulting in 204 sites for CO₂, 157 sites for CH₄ and 123 sites for N₂O globally-20, 21 and 85% more sites compared with previous global syntheses for CO₂, CH₄¹⁷ and N₂O²³, respectively. For estuary CH₄ estimates, we included primarily diffusive water-air fluxes (computed from the gas transfer velocity and the concentrations of CH₄ in water and air) and data from four studies using floating chamber incubations that estimated the total CH₄ flux (diffusive and ebullitive). The low number of total CH₄ flux estimates means that the ebullitive flux is underestimated in our analysis. particularly in the upper estuarine region. Each site/flux density was then distributed following the ten RECCAP2 regions using latitude/ longitude coordinates provided in the original studies or from Google Earth based on the study site description. Sites were categorized as either tidal systems/deltas, lagoons or fjords based on the authors' characterization of their study site. In systems for which the site description was ambiguous or not detailed enough, the type was assigned following the hierarchical steps for estuary type determination provided by Dürr et al.³¹, which are based on hydrological, lithological and morphological criteria. Estuary CO₂ and CH₄ emissions have not been modelled at global scales because of the lack of an existing spatially explicit global estuarine model designed to perform such a task. However, we supplemented the literature-derived empirical estuarine estimates of N₂O emissions with results from the spatially explicit global model from Maavara et al.²⁵. These authors used a stochastic-mechanistic model representing generalized nitrogen dynamics for water body types directly connected to river networks worldwide to extract relationships predicting N₂O emissions from water residence times and total nitrogen yields (that is, area-normalized loads) delivered to each estuary. The global total nitrogen loads were calculated using an approach inspired by Global-NEWS models⁵⁴, accounting for the nitrogen routed spatially through an inland water network joined to the estuaries indexed in Dürr et al.³¹. Emissions factors were calculated using scenarios that reflect existing literature assumptions and datasets. The model was aggregated at a spatial resolution of 0.5°, as was the case in Dürr et al.³¹ for estuary typology. Each watershed was thus assigned an estuary type based on the type of coastal cell in which the mouth of the watershed was located. Complete model details are available in Maavara et al. 25.

Coastal vegetation GHG fluxes

 $We conducted a \ literature search in Google Scholar \ and \ data \ publishers$ (FLUXNET, PANGAEA, MEMENTO and the British Oceanographic Data Centre) until the end of 2020 using the search string '(CO₂ OR CH₄ OR N₂O) AND (mangroves OR salt marshes OR seagrasses)'. Additionally, we scanned the reference lists of publications. For each site/study location (>10 km apart), we averaged spatial and seasonal variation to a single flux density, resulting in 37 sites for CO₂, 162 sites for CH₄ and 55 sites for N₂O in coastal vegetation (Extended Data Fig. 3)-15 and 42% more sites compared with previous global syntheses of coastal wetlands for CH₄¹⁷ and N₂O²³, respectively. In our global synthesis, we use only long-term eddy covariance CO₂ fluxes for coastal vegetation. We exclude chamber measurements as they do not provide information on CO₂ ecosystem exchange with a temporal coverage that is comparable to eddy covariance measurements. Although eddy covariance towers are still relatively rare in coastal vegetation, this method provides robust high-resolution long-term monthly, seasonal and often annual data of net ecosystem exchange. Eddy covariance measurements of CH₄ and N₂O are extremely rare in coastal vegetation. Therefore, we combined the few existing eddy covariance data with water-air, sediment-air, sediment-water, plant (leaf, root or stem)-air and ebullition CH₄ or N₂O fluxes where available.

CO2e GHG fluxes

For the purpose of directly comparing the relative radiative forcing effects of CO₂, CH₄ and N₂O with one another, we express GHG fluxes as CO₂e using the global warming potential for the 20-year (GWP₂₀) and 100-year (GWP₁₀₀) time horizons, including chemical adjustments reported in the Sixth Assessment Report of the IPCC⁵⁵. For CH₄, we use the non-fossil GWP₂₀ and GWP₁₀₀. Accordingly, over a 20-year time period, which is important for climate policies based on shorter time scales, 1 kg of CH₄ or N₂O has the same GWP as 79.7 or 273 kg of CO₂, respectively. Over a 100-year time period, 1 kg of CH₄ or N₂O has the same GWP as 27.0 or 273 kg of CO₂, respectively. The net contemporary GHG radiative balance for a given region, ecosystem and time horizon is the sum of the CO₂e over the three gases.

Data analyses and upscaling

Data processing and statistical analyses were performed using R software ⁵⁶. A non-parametric bootstrapping method using the package boot in R was applied to resample flux densities for each of the three gases in each of the six ecosystems (three estuary types and three coastal vegetation types) and in each of the ten RECCAP2 regions (Extended Data Fig. 4). The bootstrapping method used 1,000 iterations of the median of samples to produce a smoothed distribution of flux densities and to generate a full set of statistics. Results from non-parametric bootstrapping were then multiplied by the corresponding surface area of each of the six ecosystem types in each of the ten RECCAP2 regions. If an ecosystem type had fewer than three sites in a region, we applied the global statistics of this type in this region.

Uncertainty analysis

Uncertainties associated with flux densities were derived from the bootstrapping method that generated a full set of statistics, including Q1 and Q3 of the datasets. For estuarine surface areas, the normality of the distribution was tested successfully and allowed the derivation of upper and lower 95% confidence intervals as well as Q1 and Q3 from the standard deviation³⁰. Global mangrove forest has been mapped successfully with an overall accuracy of 99% likelihood that the true value is between 93.6 and 94.5%²⁷. The global extent of salt marshes is relatively uncertain, with recent global estimates ranging from 55,000 (ref. 28) to 90,800 km² (ref. 50). Submerged seagrasses are challenging to map and current global estimates are highly uncertain. The most recent and continuously updated global seagrass mapping effort by Short²⁹ does not estimate uncertainty. Here we assume areas per region uncertainty of 5, 10 and 20% for mangroves, salt marshes and seagrasses, respectively, noting that these uncertainties could be substantially larger for the latter two types of coastal vegetation. We then combine the respective uncertainties of GHG flux densities with uncertainties of surface area of either estuaries or coastal vegetation using the root sum of the squares method, which calculates the square root of the linear sum of the squared standard uncertainty components, treating the uncertainty contributors as statistically independent. We present the combined uncertainties of Q1 and Q3 in accordance with the median in the main article because this statistical set represents the most appropriate measure of the non-normally distributed GHG fluxes.

Reporting summary

Further information on research design is available in the Nature Portfolio Reporting Summary linked to this article.

Data availability

All of the data included in this study are freely available at https://doi.org/10.6084/m9.figshare.22351267. These data may be used if cited appropriately.

References

 Gillies, S., Ward, B., & Petersen, A. S. Rasterio. GitHub https://github.com/mapbox/rasterio (2013).

- 53. Jordahl, K. et al. Geopandas/geopandas: v0.8.1. *Zenodo* https://doi.org/10.5281/zenodo.3946761 (2020).
- Mayorga, E. et al. Global Nutrient Export from WaterSheds 2 (NEWS 2): model development and implementation. *Environ*. *Model*. Softw. 25, 837–853 (2010).
- Forster, et al. in Climate Change 2021: The Physical Science Basis (eds Masson-Delmotte, V. et al.) 923–1054 (Cambridge Univ. Press. 2021).
- R Core Development Team. R: A Language and Environment for Statistical Computing (R Foundation for Statistical Computing, 2020).

Acknowledgements

We thank the RECCAP2 Scientific Committee and members of the Global Carbon Project who initiated this group effort (https://www. globalcarbonproject.org/reccap/index.htm). We thank the following members of the AmeriFlux site teams who contributed annual net ecosystem CO2 exchange sums for their sites: E. Stuart-Haëntjens, B. Bergamaschi, L. Windham-Myers, A. Vázquez-Lule, R. Vargas, J. Shahan, P. Oikawa, P. Hawman, D. Mishra, R. Sanders-DeMott and P. Polsenaere. J.A.R. and T.M. acknowledge funding from the Hutchinson Postdoctoral Fellowship of the Yale Institute for Biospheric Studies at Yale University. I.F. acknowledges the National Science Foundation Long Term Ecological Research program (OCE 1637630). R.G.N. acknowledges support from the National Aeronautics and Space Administration's Carbon Cycle Science Program. G.G.L. is a research associate of the F.R.S.-FNRS at the Université Libre de Bruxelles. P.R. received financial support from the Belgian Science Policy Office (through the project ReCAP, which is part of the Belgian research program FedTwin), the European Union's Horizon 2020 research and innovation program ESM2025—Earth System Models for the Future project (grant number 101003536) and the F.R.S.-FRNS PDR project T.0191.23. B.D.E. acknowledges support from Australian Research Council grants DP220100918, LP200200910 and LP190100271. W.-J.C. acknowledges support from the National Oceanic and Atmospheric Administration and National Science Foundation. J.J.M.B. acknowledges the computational resources provided by Princeton Institute for Computational Science and Engineering, which were used for the land segmentation. B.V.D. was supported by the Bundesministerium für Bildung und Forschung project CARBOSTORE (number 03F0875A), as well as the German Academic Exchange Service project 'The ocean's alkalinity: connecting geological and metabolic processes and time-scales' (number 57429828).

Author contributions

J.A.R. and P.R. conceived of and designed the study. J.A.R. performed the synthesis for CH $_4$ and N $_2$ O in estuaries, CH $_4$ and N $_2$ O in coastal vegetation and CO $_2$ in mangroves. B.D.E. and H.W.B. helped with the synthesis for N $_2$ O in estuaries and coastal vegetation. T.M. provided the mechanistic model for N $_2$ O in estuaries. G.G.L. performed the synthesis for CO $_2$ in estuaries and segmented the estuarine surface area. I.F. performed the synthesis for CO $_2$ in salt marshes. B.V.D. performed the synthesis for CO $_2$ in seagrasses. J.J.M.B. segmented the coastal vegetation surface area. J.A.R. produced the results and figures and wrote the original draft of the paper. All authors helped with interpretation of the data and contributed to reviewing and editing the paper.

Competing interests

The authors declare no competing interests.

Additional information

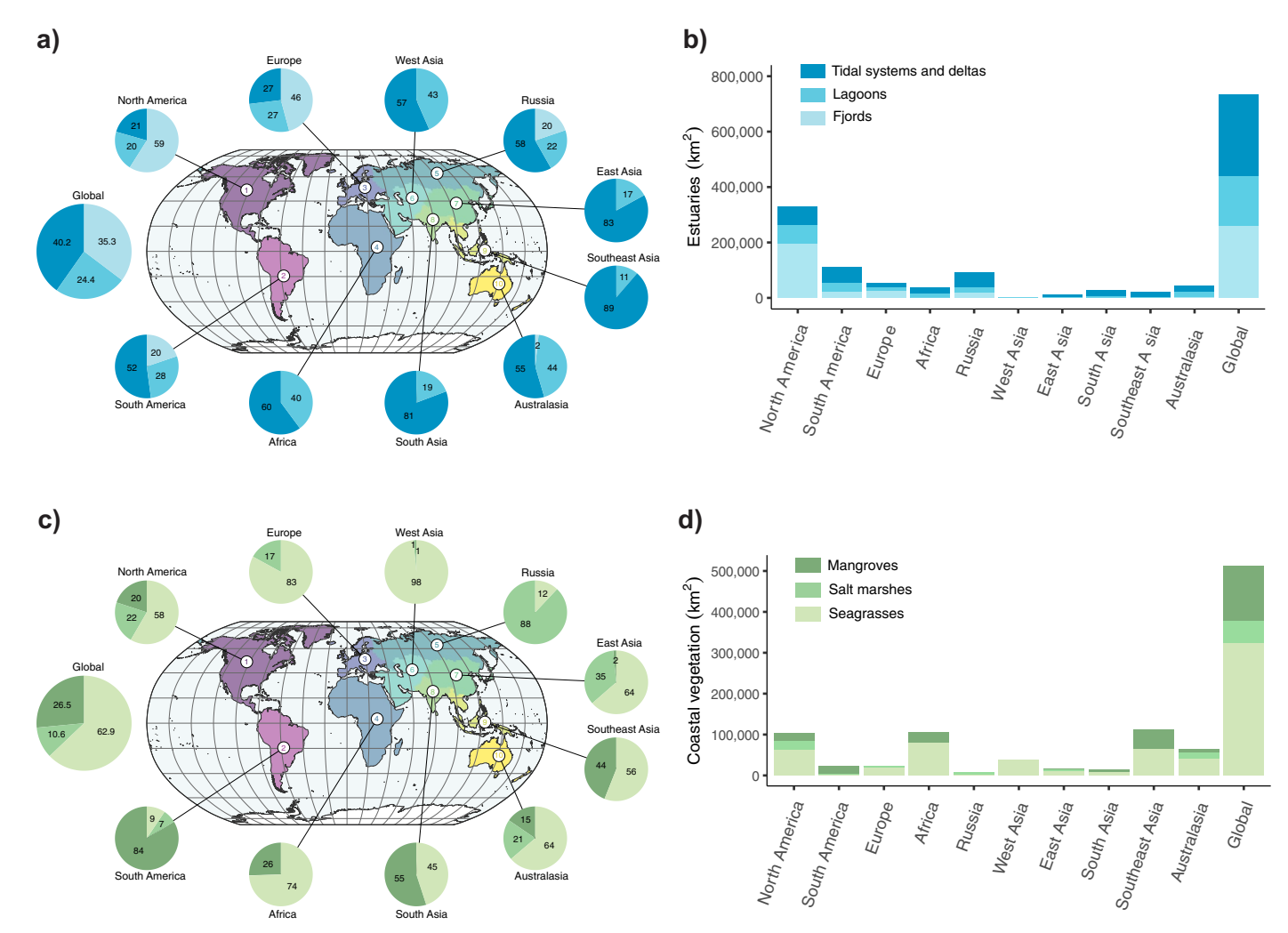
Extended data is available for this paper at https://doi.org/10.1038/s41558-023-01682-9.

Supplementary information The online version contains supplementary material available at https://doi.org/10.1038/s41558-023-01682-9.

Correspondence and requests for materials should be addressed to Judith A. Rosentreter.

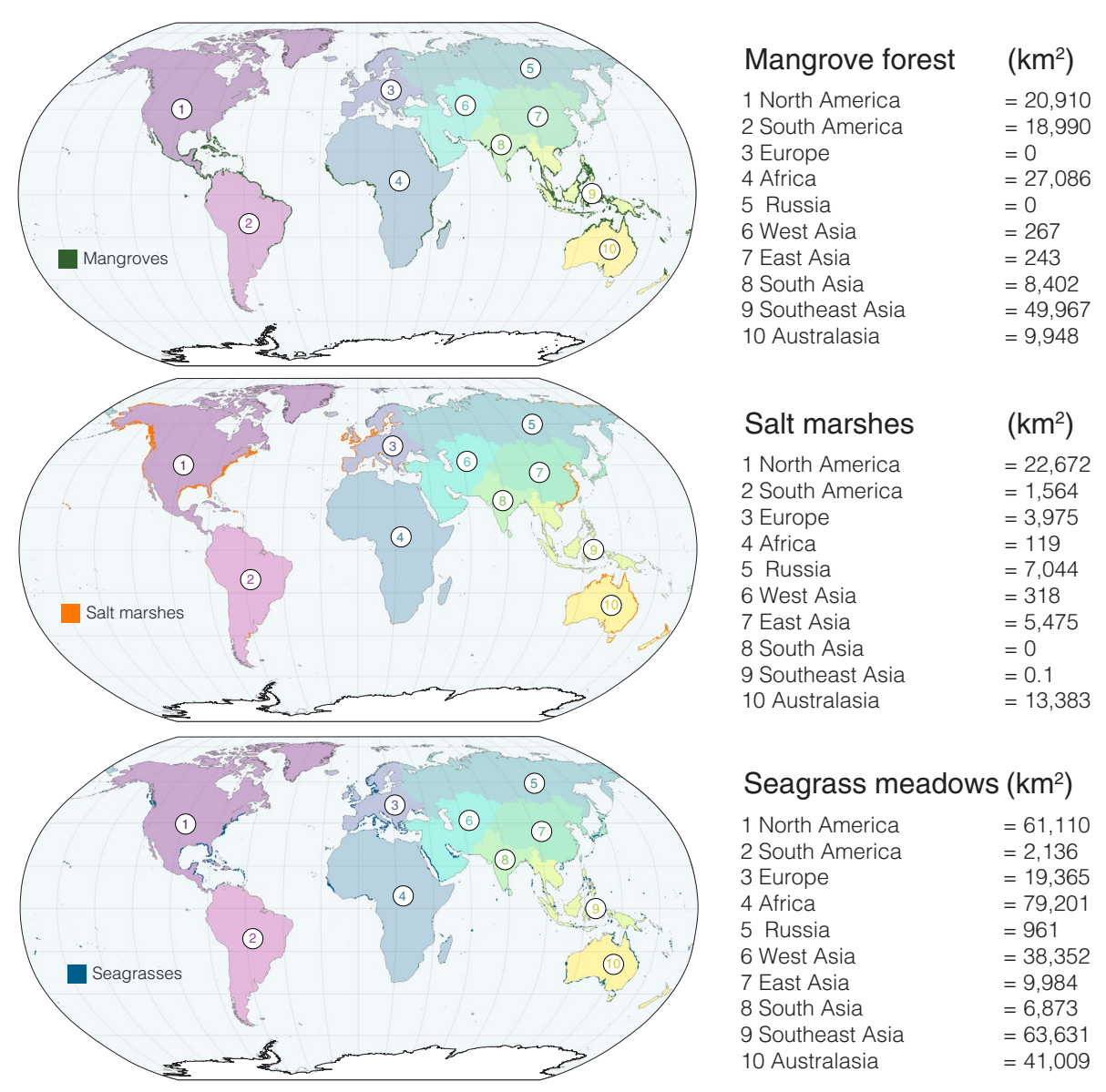
Peer review information *Nature Climate Change* thanks Shuwei Li, James Megonigal, Dongqi Wang and Cathleen Wigand for their contribution to the peer review of this work.

Reprints and permissions information is available at www.nature.com/reprints.

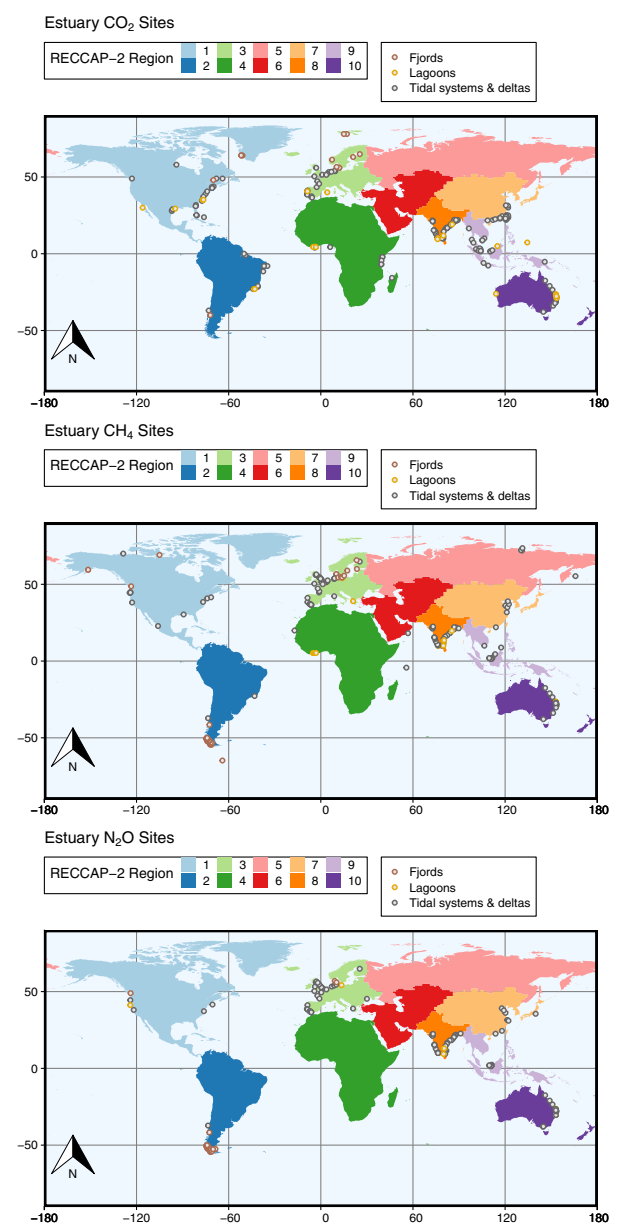


Extended Data Fig. 1| **Regional and global surface areas of estuaries and coastal vegetation.** Surface areas of estuaries a) as a relative percentage (%) and b) in km² of tidal systems and deltas, lagoons, and fjords in the ten RECCAP2 regions and globally. Surface areas of coastal vegetation c) as a relative percentage (%) and d) in km² of mangroves, salt marshes, and seagrasses in

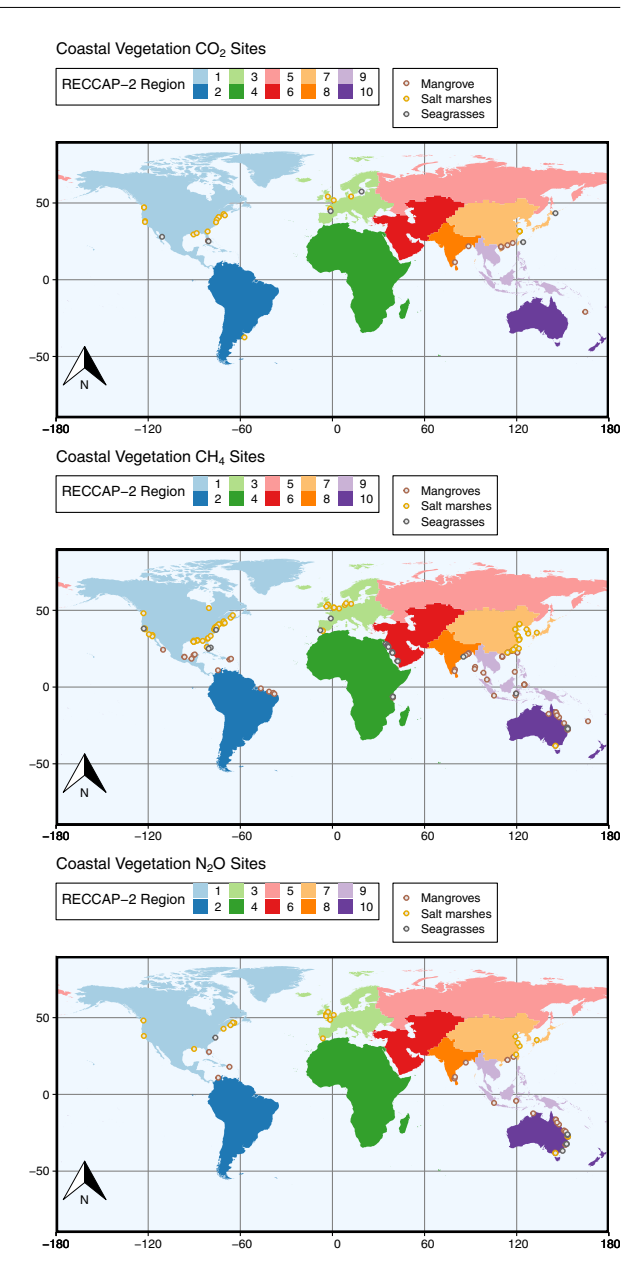
the ten RECCAP2 regions and globally. The global surface area for estuaries is 733,801 km²³³0. The global coastal vegetation area is 512,982 km². Surface areas (km²) for each estuary and coastal vegetation type in each of the ten regions can be found in Supplementary Table S4.



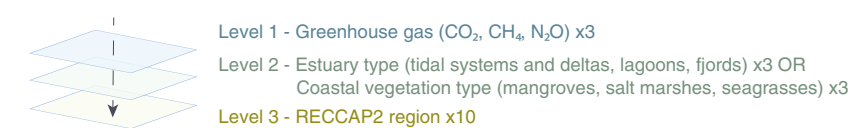
Extended Data Fig. 2 | **Distribution of regional coastal vegetation.** Map showing the ten RECCAP2 regions and coastal vegetation distribution of mangrove forest, salt marshes, and seagrass meadows. To the right: regional surface areas (km²) of mangroves, salt marshes, and seagrasses in the ten RECCAP2 regions. Data from refs. 27,28,29.



Extended Data Fig. 3 | Greenhouse gas study site locations in estuaries and coastal vegetation. Map showing locations of CO_2 , CH_4 , and N_2O flux studies in the ten RECCAP2 regions in estuaries (left side): tidal systems and deltas, lagoons,



and fjords, and coastal vegetation (right side): mangroves, salt marshes, and seagrasses, from peer-reviewed publications until the end of 2020. The number of study sites can be found in Supplementary Table S8.



 $\textbf{Extended Data Fig. 4} | \textbf{Bootstrapping approach.} \\ \textbf{Bootstrapping was applied to randomly resample flux densities of the three greenhouse gases (level 1) for each estuary or coastal vegetation types (level 2) for each of the ten RECCAP2 regions (level 3) before upscaling to specific surface areas (see Supplementary Table S4).}$

nature portfolio

Corresponding author(s):	Judith Rosentreter
Last updated by author(s):	Apr 14, 2023

Reporting Summary

Nature Portfolio wishes to improve the reproducibility of the work that we publish. This form provides structure for consistency and transparency in reporting. For further information on Nature Portfolio policies, see our <u>Editorial Policies</u> and the <u>Editorial Policy Checklist</u>.

_				
· ·	トつ	.+-	-	ics
	_		151	11 5

For	all statistical an	alyses, confirm that the following items are present in the figure legend, table legend, main text, or Methods section.
n/a	Confirmed	
	The exact	sample size (n) for each experimental group/condition, given as a discrete number and unit of measurement
\boxtimes	A stateme	nt on whether measurements were taken from distinct samples or whether the same sample was measured repeatedly
	The statist Only comm	cical test(s) used AND whether they are one- or two-sided on tests should be described solely by name; describe more complex techniques in the Methods section.
\boxtimes	A descript	ion of all covariates tested
	A descript	ion of any assumptions or corrections, such as tests of normality and adjustment for multiple comparisons
	A full desc	ription of the statistical parameters including central tendency (e.g. means) or other basic estimates (e.g. regression coefficient) tion (e.g. standard deviation) or associated estimates of uncertainty (e.g. confidence intervals)
\boxtimes	For null hy Give P value	pothesis testing, the test statistic (e.g. F , t , r) with confidence intervals, effect sizes, degrees of freedom and P value noted as as exact values whenever suitable.
\boxtimes	For Bayesi	an analysis, information on the choice of priors and Markov chain Monte Carlo settings
\times	For hierar	chical and complex designs, identification of the appropriate level for tests and full reporting of outcomes
\boxtimes	Estimates	of effect sizes (e.g. Cohen's d , Pearson's r), indicating how they were calculated
		Our web collection on <u>statistics for biologists</u> contains articles on many of the points above.
So	ftware and	d code
Poli	cy information a	about <u>availability of computer code</u>
Da	ata collection	Data were extracted from peer-reviewed publications searching in Google Scholar, and data publishers: Fluxnet, MEMENTO, PANGAEA, British

Data analysis was performed using R (R Core Team, version 4.0.3, 2020). A non-parametric bootstrapping method was performed using the

Data

Data analysis

Policy information about availability of data

All manuscripts must include a <u>data availability statement</u>. This statement should provide the following information, where applicable:

For manuscripts utilizing custom algorithms or software that are central to the research but not yet described in published literature, software must be made available to editors and reviewers. We strongly encourage code deposition in a community repository (e.g. GitHub). See the Nature Portfolio guidelines for submitting code & software for further information.

- Accession codes, unique identifiers, or web links for publicly available datasets
- A description of any restrictions on data availability
- For clinical datasets or third party data, please ensure that the statement adheres to our policy

The datasets that support the findings of this study are available in the Figshare repository: 10.6084/m9.figshare.22351267

package boot. Plots were generated using ggplot2 package and Adobe Illustrator.

Human research participants							
Policy information about stu	dies involving human research participants and Sex and Gender in Research.						
Reporting on sex and gend	der NA						
Population characteristics	NA						
Recruitment	NA						
Ethics oversight	NA						
Note that full information on th	e approval of the study protocol must also be provided in the manuscript.						
Field-specific	reporting						
Please select the one below	that is the best fit for your research. If you are not sure, read the appropriate sections before making your selection.						
Life sciences	Life sciences Behavioural & social sciences Ecological, evolutionary & environmental sciences						
For a reference copy of the docume	nt with all sections, see <u>nature.com/documents/nr-reporting-summary-flat.pdf</u>						
Ecological, ev	olutionary & environmental sciences study design						
All studies must disclose on	these points even when the disclosure is negative.						
Study description	Meta-analysis of coastal greenhouse gas fluxes (CO2, CH4, N2O)						
Research sample	Literature search of peer-reviewed publications until end of 2020						
Sampling strategy	Boolean search string to search for publications in databases. Additionally, we scanned the reference lists of publications.						
	Data were extracted using Microsoft Excel. JAR did the synthesis for CH4 and N2O in estuaries, and for CH4 and N2O in coastal vegetation. BDE and HWB helped with in the synthesis for N2O in estuaries and coastal vegetation. GGL did the synthesis for CO2 in estuaries. IF did the synthesis for CO2 in salt marshes. BVD did the synthesis for CO2 in seagrasses. JAR did the synthesis for CO2 in mangroves.						
Timing and snatial scale	Database includes studies published in the years 1975-2020						

Reporting for specific materials, systems and methods

with salinity < 0.5, chamber studies for coastal vegetation CO2 flux datasets.

The database containing compiled data sets is accessible via figshare.

mangroves, 2) salt marshes, 3) seagrasses

No.

No blinding strategy

Data exclusions

Reproducibility

Randomization

Did the study involve field work?

Blinding

We require information from authors about some types of materials, experimental systems and methods used in many studies. Here, indicate whether each material, system or method listed is relevant to your study. If you are not sure if a list item applies to your research, read the appropriate section before selecting a response.

See Methods and Supplementary Information for coastal ecosystem definitions. Data were included if sites met these definitions. In

brief, we excluded greenhouse gas flux data from freshwater marsh, tidal rivers, mudflats and bare sediments, coastal ecosystems

Estuary data was grouped into 1) tidal systems and deltas, 2) lagoons, 3) fjords. Coastal vegetation data was grouped into 1)

Materials & experimental systems Methods n/a Involved in the study n/a Involved in the study ☑ Antibodies ☑ ChIP-seq ☑ Eukaryotic cell lines ☑ Flow cytometry ☑ Palaeontology and archaeology ☑ MRI-based neuroimaging ☑ Animals and other organisms ☑ Clinical data

Dual use research of concern